



## 1 Saturated and unsaturated salt transport in peat from a constructed 2 fen

3 Reuven B. Simhayov<sup>1</sup>, Tobias K. D. Weber<sup>1,2</sup>, Jonathan S. Price<sup>1</sup>

4 <sup>1</sup>Department of Geography, University of Waterloo, Waterloo, Ontario, N2L 3G1, Canada

5 <sup>2</sup>Soil Science and Soil Physics Division, Institute of Geoeology, TU Braunschweig, Langer Kamp 19c, 38106  
6 Braunschweig, Germany

7

8 *Correspondence to:* Reuven B. Simhayov ([rbsimhay@uwaterloo.ca](mailto:rbsimhay@uwaterloo.ca))

9 **Abstract.** To determine the underlying processes of solute transport in peat an experimental constructed fen peatland, soil  
10 hydraulic properties were measured and saturated and unsaturated solute breakthrough experiments were performed using  
11 Na<sup>+</sup> and Cl<sup>-</sup> as reactive and non-reactive solutes, respectively. We tested the performance of three solute transport models,  
12 including the classical equilibrium Convection-Dispersion Equation (CDE), a chemical non equilibrium one-site adsorption  
13 model (OSA) and a model to account for physical non-equilibrium, the mobile-immobile phases (MIM). The selection was  
14 motivated by the fact that the applicability of the MIM in peat soils finds a wide consensus. However, results from inverse  
15 modelling and a robust statistical evaluation of this peat provide evidence that the measured breakthrough of the  
16 conservative tracer, Cl<sup>-</sup> could be simulated well using the CDE. This is demonstrated by a very high Damköhler number  
17 ( $\rightarrow$ infinity) suggesting instantaneous equilibration between the mobile and immobile phases; this underscores the  
18 redundancy of the MIM approach for this particular peat. Scanning electron microscope images of the peat show the typical  
19 multi-pore size distributions structure have been homogenised sufficiently by decomposition, such that physical non-  
20 equilibrium solute transport no longer governs the transport process. This is corroborated by the fact the soil hydraulic  
21 properties were adequately described using a unimodal van Genuchten-Mualem model between saturation and a pressure  
22 head of  $\sim$  -1000 cm of water. Hence, MIM is not the most suitable choice, and the long tailing of the Na<sup>+</sup> breakthrough curve  
23 is caused by chemical non-equilibrium. Successful description was possible using the OSA model. To test our results for the  
24 unsaturated case, we conducted an unsaturated steady state evaporation experiment to drive Na<sup>+</sup> and Cl<sup>-</sup> transport. Using the  
25 parameterised transport models from the saturated experiments, we could numerically simulate the unsaturated transport  
26 using Hydrus-1D. The simulation showed a good prediction of observed values, confirming the suitability of the parameters  
27 for use in a slightly unsaturated transport simulation. The findings improve the understanding of solute redistribution in the  
28 constructed fen.

29

30 **Keywords:** solute transport, peat, non-equilibrium, unsaturated,



## 31 1 Introduction

32 The incorporation of large quantities of tailings sand into a constructed fen watershed created as part of a novel attempt at  
33 landscape reclamation in the oil sands region, introduced a large pool of leachable Na, Ca and S (Simhayov et al., 2017).  
34 Near surface accumulation and potential impact of these solutes on the vegetation is controlled by the transport rate from the  
35 upland to the fen and the rate of flushing out of the system, which are currently under investigation (Simhayov et al., 2017).  
36 In constructed peatlands designed for oil sands reclamation landscapes, water quality is a concern due to incorporation of  
37 process-affected materials (Price et al., 2011; Daly et al., 2012). In this context a better understanding of the transport  
38 processes through peat and solute accumulation in the rooting zone of the fen is needed.

39 The current assumption is that solute attenuation in peat is a result of mass exchanges between mobile and immobile phases  
40 (Hoag and Price, 1997; Rezaeehad et al., 2012). Generally, *Sphagnum* derived peat, hyaline cells and their skeletal  
41 remnants are thought to account for a large fraction of dead end pores with distinct pore size density distributions (Weber et  
42 al., 2017a, 2017b) and a volumetric moisture content (VMC) between 10 and 20% (Hayward and Clymo, 1982; Weber et al.,  
43 2017a; 2017b). Additionally, surface adsorption of reactive solutes (Rezaeehad et al., 2012; 2016) may be present. Both  
44 effects lead to more dilute but longer solute plumes which might affect revegetation efforts in oil sands reclamation  
45 landscapes. The physical and hydraulic properties of undisturbed peat changes along a continuous vertical profile (Weber et  
46 al. 2017b, Limpens et al. 2008), whereby deep peat layers are generally more decomposed (Clymo, 1983). In addition to  
47 pore-scale effects, the systematic layered heterogeneity common in natural peatlands influences mixing and transport (Hoag  
48 and Price, 1995). However, in constructed peatlands this is destroyed because of the disruption caused by stripping, transport  
49 and placement (Nwaishi et al., 2015).

50

51 Solute transport in the subsurface may be subject to physical and chemical non-equilibrium (Nielsen et al., 1986)  
52 invalidating the use of the conventional convection dispersion equation (CDE) to simulate it. Physical non-equilibrium is  
53 thought to be a process of a heterogeneous flow field with spatial differences in hydraulic conductivity due to dead-end pores  
54 (Coats and Smith, 1964, Zurmühl and Durner, 1996), non-moving intra-aggregate water (Philip, 1968; Passioura, 1971), or  
55 stagnant water in thin liquid films around soil particles (Nielsen et al. 1986). In this mobile-immobile model (MIM, Coats  
56 and Smith, 1964; van Genuchten and Wierenga, 1976) the liquid phase is partitioned into a mobile and an immobile region.  
57 Convective-dispersive transport occurs only in the mobile zone, while solute transport into the immobile region is by  
58 diffusion, the rate of which can be determined by experiments and inverse estimation of transport parameters (Vanderborght  
59 et al., 1997). In chemical non-equilibrium models, it is assumed that sorption at the pore-water solid particle interface is  
60 kinetically controlled (Cameron and Klute, 1977; Nkedi-Kizza et al. 1989). Both parametric non-equilibrium models may  
61 additionally account for chemical equilibrium adsorption (Toride et al. 1993).

62 To distinguish between the governing solute transport process, inverse modelling can provide the necessary information on  
63 model parameter estimates, associated uncertainties, and permits the calculation of model performance and selection criteria



64 (Iden and Durner, 2008; Vrugt and Dane, 2005, Weber et al. 2017). This can be based on measured solute breakthrough  
65 experiments of reactive as well as non-reactive solutes (Nkedi-Kizza et al., 1984). In the notation of the convection  
66 dispersion equation the retardation factor is strictly referred and attributed to equilibrium adsorption (Toride et al., 1995,  
67 Šimůnek and van Genuchten, 2008, Šimůnek et al. 2008) and is a function of bulk density, the slope of the adsorption  
68 isotherm, and volumetric water content (Toride et al., 1995). A problem in deriving a numerical value for the retardation  
69 factor during inverse modelling is that it is mathematical directly negatively proportional to the flow.

70 To date the only literature reports with experiments of NaCl breakthrough on saturated peat columns conducted in the  
71 laboratory are from Price and Woo (1988), Ours et al. (1997), Hoag and Price (1997) and Rezanezhad et al. (2012). Ours et  
72 al. (1997) speculate that the observed prolonged tailing of NaCl is a result of solutes diffusing into immobile zones.  
73 However, neither batch adsorption tests with the potential to exclude kinetic chemical sorption are presented, nor were solute  
74 transport models fitted to breakthrough curves, leaving their conclusions tentative. Hoag and Price (1997) successfully  
75 described their observations with the conventional convection dispersion equation (CDE). However, based on an effective  
76 porosity ( $n_e$ ) determined by photo imagery the authors calculated the calculate pore water velocity by  $v = q/n_e$ , where  $q$  is  
77 specific discharge. This results in higher values of  $v$  than those calculated from total porosity,  $\phi$ , or inverse estimation. By  
78 estimating CDE model parameters describing non-reactive Cl<sup>-</sup> breakthrough and keeping  $v$  fixed, their retardation factor ( $R$ ),  
79 reflecting  $v_{water}/v_{solute}$  was  $>1$ , and close to the ratio of  $\phi$  to  $n_e$ . They attributed the delay in solute transport to physical  
80 non-equilibrium processes, whereby solutes diffuse into inactive pores (i.e. solute transfer from the mobile to the immobile  
81 region). The approach of Hoag and Price (1997) differs from the classical understanding where diffusion into the immobile  
82 zone is described by a kinetic constant, while  $R$  assumes chemical equilibrium of solutes with sorption sites (e.g. Coats and  
83 Smith, 1964; van Genuchten and Wierenga, 1976). Rezanezhad et al. (2012) concluded MIM transport is observable on  
84 small peat samples Moreover, parameter uncertainties and correlations are not shown and the performance of the MIM in  
85 comparison to the classical CDE is not given such that a rigorous model selection is not possible.

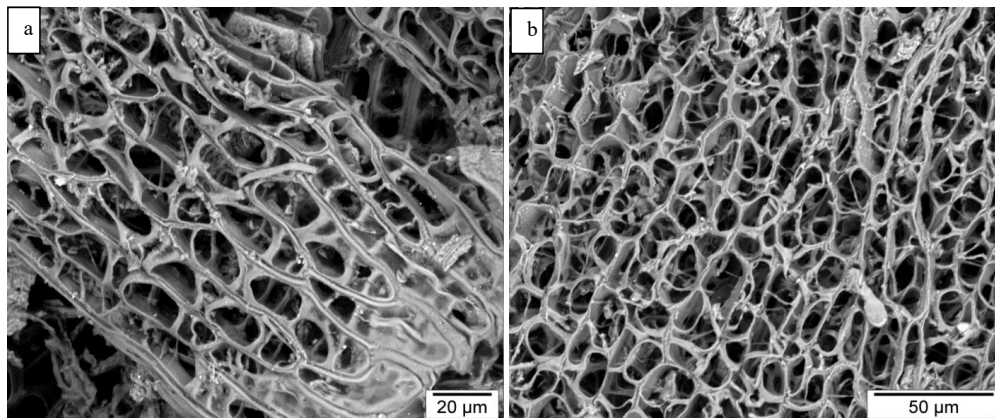
86 The goal of the study is to expand our understanding of the transport processes in the vadose zone of decomposed peat by  
87 testing various transport models and scrutinizing the common assumption that the mobile-immobile transport model best  
88 reflects the processes in saturated and unsaturated peat. We approach this by conducting saturated breakthrough experiments  
89 using NaCl. Cl<sup>-</sup> is generally uninvolved in chemical reactions in peat, except for ultra-saline conditions (Ours et al., 1997),  
90 and its counter-ion, Na<sup>+</sup>, is a prominent solute and potential contaminant in the oil sands reclamation landscape (Simhayov et  
91 al., 2017). To compare the performance of models, model parameters were estimated using inverse modelling with the  
92 CXTFIT v2.0 code (Toride et al. 1995). Comparison was based on a statistical analysis to investigate the information content  
93 of the data collected, enabling a careful assessment of the underlying processes. Subsequently, the parameterised models  
94 were used to numerically simulate the solute transport in unsaturated steady state evaporation experiments with Hydrus-1D  
95 (Simunek et al., 2008). We tested if the model selection and parameterization based on saturated experiments can be  
96 extended to predict unsaturated solute transport. No further inverse estimation was done for the unsaturated transport of the  
97 non-reactive solute except for the Freundlich-Langmuir parameters of the reactive solute. A sensitivity analyses was then



98 carried out to estimate potential errors caused by using parameters derived from saturated transport to simulate the  
99 unsaturated case.

## 100 2 Materials and methods

101 The peat used for the fen was moderately decomposed rich fen, sedge peat, taken from a donor fen prior to stripping the  
102 overburden material to expose the oil sands deposits (Price et al., 2011; Daly et al., 2012; Nwaishi et al., 2015). Peat samples  
103 were taken from a donor fen prior to stripping the overburden material to expose the oil sands deposits (Price et al., 2011;  
104 Daly et al., 2012; Nwaishi et al., 2015). The donor fen had been drained for two years prior to stripping and the peat  
105 underwent rapid decomposition due to exposure to oxygen (Nwaishi et al., 2015). The peat has a relatively open structure  
106 (Fig. 1), compared to *Sphagnum* peat used in other transport studies (e.g. Hoag and Price, 1989; Rezanezhad et al., 2012).  
107



108  
109 **Figure 1 – Scanning electron microscope pictures of samples of the peat used in this study. a) Moss with hyaline cells,**  
110 **note cells with intact membrane at bottom right corner and larger pore spaces in bottom left and top right corners. b)**  
111 **Moss cells, Note that membranes are missing and a view through the skeleton is evident. Modified from Rezanezhad**  
112 **et al., (2016)**

### 113 2.1 Research approach

114 Four soil physical experiments were conducted to estimate the hydraulic properties and solute transport characteristics of the  
115 fen peat material. The conducted experiments were: 1) Transient evaporation; 2) Water retention characteristics using  
116 tension disks; 3) Saturated breakthrough; and 4) Unsaturated breakthrough. Initially, the peat was cleaned from woody plant



117 material such as leaves and stems, to increase replicability. Furthermore, to reduce variations in moisture content between  
118 samples, the peat was thoroughly mixed before a sample was packed (see appendix A.1). Prior to experimentation samples  
119 were saturated from the bottom in small increments, over a 24-hour period, using 18.2M $\Omega$ ·cm water (ultra-pure water). All  
120 experiments were conducted at a target bulk density, ( $\rho_B$ ; g cm<sup>-3</sup>), of 0.12. Experiments were conducted in triplicates, except  
121 for the tension disk experiments, which were conducted on 4 samples. For the determination of the solute transport  
122 properties, Cl<sup>-</sup> was used as a non-reactive solute and Na<sup>+</sup> as a reactive solute. All breakthrough experiments were performed  
123 using a solution of 200 mg l<sup>-1</sup> Na<sup>+</sup> and 300 mg l<sup>-1</sup> Cl<sup>-</sup> corresponding to values measured by Kessel (2016) in the constructed  
124 Nikanotee Fen watershed. This solution was prepared by mixing 500 mg of NaCl (1.06404.055, ACS grade, Merck,  
125 Germany) per 1 l of ultra-pure water.

## 126 2.2 Soil hydraulic properties

127 To determine the peat soil hydraulic properties, we conducted transient evaporation experiments (Schindler, 1980, Peters et  
128 al., 2015, Weber et al., 2017a, 2017b) for the retention properties, supplemented with tension disk experiments (Klute and  
129 Dirksen, 1986; McCarter et al., 2017). Tension disk experiments are considered to be a more reliable method to determine  
130 the unsaturated hydraulic conductivity in the wet range, because transient evaporation experiments contain limited  
131 information at pressures heads between 0 and -60 cm for the unsaturated hydraulic conductivity curve (Peters and Durner,  
132 2008). Water retention and unsaturated hydraulic conductivity data were obtained with the tension disk experiments using 10  
133 cm i.d. and 5 cm high peat samples at -2.5, -5, -7.5, -10, -15, -20, -25 cm pressure head (h; cm) steps, which was also the  
134 order in which the experiment was conducted. Outflow during each pressure step was monitored by scales with an accuracy  
135 of 0.1 g and logged at 1-minute intervals and the unsaturated hydraulic conductivity calculated with the Darcy-Buckingham  
136 equation (Swartzendruber, 1969). The transient evaporation experiments were conducted on the same samples using  
137 commercial UMS HYPROP devices (UMS GmbH, Munich, Germany). The water retention and unsaturated hydraulic  
138 conductivity data were then used to obtain parameters of the unimodal van Genuchten-Mualem model (van Genuchten,  
139 1980; Mualem, 1976) by inverse modelling. For further details on parameters the reader is referred to appendix A.2.

140 The volumetric water content,  $\theta$ , was determined as the difference between sample weight and the oven-dry mass for  
141 samples dried at 80°C until no difference in weight was measured (Gardner, 1986). Bulk density was determined as the ratio  
142 of dry weight to the original sample volume. Volumetric water content at saturation,  $\theta_s$ , was assumed to be equivalent to the  
143 sample total porosity. Saturated hydraulic conductivity ( $K_s$ ; cm d<sup>-1</sup>) was determined with a constant head test (Freeze and  
144 Cherry, 1979) using the flow-through chambers described below and a hydraulic gradient of 1.



145 **2.3 Saturated breakthrough experiments and inverse modelling**

146 **2.3.1 Sample preparation**

147 Saturated breakthrough experiments were conducted in 10 cm long, 10 cm i.d. Plexiglas™ (785 cm<sup>3</sup>) flow-through  
 148 chambers, fitted at each end with 2.5x15x15 cm HDPE end-plates with silicon gaskets. A polypropylene fibre pad was  
 149 placed between the plate and the sample to enhance the distribution of the solution beneath the sample (see appendix A.1).  
 150 The NaCl solute source was a 20 l magnetically stirred solution reservoir pumped at a steady rate of 5 ml min<sup>-1</sup> (a flux  
 151 density of 0.064 cm min<sup>-1</sup>) using a peristaltic pump (WT600-3J, LongerPump, China) and the outflow solute concentration  
 152 monitored continuously (e.g. Skaggs and Leij, 2002). Prior to the breakthrough experiment, the samples were flushed with 2  
 153 chamber volumes of the NaCl solution to reduce potential changes to the pore sizes as a result of swelling (Price and Woo,  
 154 1988; Ours et al., 1997) or clogging due to flocculation. Subsequently, the samples were inverted and flushed with ultra-pure  
 155 water for 6 chamber volumes to remove the solutes that were introduced. To determine sampling times and the end of the  
 156 experiment an EC electrode (11388-372, SympHony, VWR, USA) connected to a portable meter (SP80PC, SympHony,  
 157 VWR, USA) was used. The EC meter was calibrated using a 2-point calibration with 84 μS cm<sup>-1</sup> and 1413 μS cm<sup>-1</sup>  
 158 conductivity calibration solutions (HI-7033 and HI-7031, respectively (Hanna instruments, USA)). EC was checked every 5-  
 159 10 minutes depending on the trend observed. Sampling was done with observed changes in EC and the experiment was  
 160 continued until 1 hour after the outflow EC value was similar to the inflow. Samples were collected in 1.5 ml polypropylene  
 161 micro centrifuge tubes (Z336769, Sigma Aldrich, USA) and kept frozen until analysed. Water samples were analysed for  
 162 Na<sup>+</sup> and Cl<sup>-</sup> using an ion chromatograph (IC) (DIONEX ICS 3000, IonPac AS18 and CS16 analytical columns). Apparatus  
 163 blank corrections were done as described in Rajendran et al. (2008), where no transport model for the apparatus blank was  
 164 assumed but correction values generated using hermite cubic splines.

165 **2.3.2 Solute transport models**

166 Two different parametric solute transport model types were used to describe the observed breakthrough data of Cl<sup>-</sup> and a  
 167 third additional model for the Na<sup>+</sup> data. We list the model in the order of testing. The first two consisted of the mobile  
 168 immobile equation (MIM; Eq. (1) and (2); van Genuchten and Wagenet, 1989) and the classical convection dispersion  
 169 equation (CDE; Eq. (3); van Genuchten and Alves, 1982, Nielsen et al., 1986), and the third is the one-site adsorption  
 170 equation (OSA; Eq. (5) and (6); van Genuchten et al., 1974, Nielsen et al., 1986) which was only used for Na<sup>+</sup>.

171 The MIM for a non-reactive solute with instantaneous equilibration is given by

172

$$\beta\theta \frac{\partial c_m}{\partial t} = D \frac{\partial^2 c_m}{\partial x^2} - v \frac{\partial c_m}{\partial x} - \alpha_{MIM}(c_m - c_{im}) \quad \text{Eq. (1)}$$

$$(1 - \beta)\theta \frac{\partial c_{im}}{\partial t} = \alpha_{MIM}(c_m - c_{im}) \quad \text{Eq. (2)}$$



173 where  $\beta$  is the ratio of the water content of the mobile region to the total water content,  $\theta$  ( $L^3 L^{-3}$ ),  $C_m$  and  $C_{im}$  are the  
 174 concentrations in the water phase of the mobile and immobile regions ( $M/L^3$ ), respectively,  $D$  is the dispersion coefficient  
 175 ( $L^2 T^{-1}$ ),  $v$  is the average linear pore water velocity ( $L T^{-1}$ ), and  $\alpha_{MIM}$  is the first order rate coefficient between the mobile  
 176 and immobile region ( $T^{-1}$ ).

177 The CDE is given by

178

$$\frac{\partial c}{\partial t} = \frac{D}{R} \frac{\partial^2 c}{\partial z^2} - \frac{v}{R} \frac{\partial c}{\partial z} \quad \text{Eq. (3)}$$

179

180 where  $c$  is the concentration of the total water phase ( $M L^{-3}$ ), and  $R$  is a retardation factor for equilibrium adsorption, which  
 181 for a non-reactive solute is typically assumed to be 1 (but see Hoag and Price, 1997). In the classical interpretation,  $R$  is  
 182 related to the adsorption distribution coefficient,  $K_d$  ( $M^3 L^{-3}$ ), by  $R = 1 + \rho_B K_d / \theta$ . The MIM reduces to the CDE  
 183 equation under certain conditions, which can be analysed by the dimensionless Damkohler number ( $D_a$ ; Vanderborght et  
 184 al., 1997, Wehrer and Totsche, 1995), Eq. (4), given by

185

$$D_a = \frac{\alpha_{MIM} L}{v(1 - \beta)\theta} \quad \text{Eq. (4)}$$

186

187 where  $L$  is the column length ( $L$ ). Large  $D_a$  values indicate very fast equilibration between the regions. From inspection of  
 188 Eq. (4) it becomes clear that  $\lim_{\beta \rightarrow 1} D_a \rightarrow \infty$ , and as  $\alpha_{MIM}$  increases,  $D_a$  increases proportionally, signifying instantaneous  
 189 equilibration, thus a differentiation between the two regions cannot be determined. Moreover, Parker and Valocchi (1986)  
 190 showed that the CDE may also be applicable when a considerable part of the solute dispersion is caused by diffusion into the  
 191 immobile region.

192 In physical non-equilibrium the attenuation of both reactive and non-reactive solutes is affected. However, if only the  
 193 reactive solute shows long tailing, then it can be assumed that chemical non-equilibrium is affecting the flow process. In  
 194 NaCl breakthrough experiments (Rezanezhad et al., 2012), only  $Na^+$  showed long tailings in fen peat so that the physical  
 195 non-equilibrium model should not be employed. For this case, first-order kinetic chemical non-equilibrium models may be  
 196 chosen. One typical model for solute transport in porous media is the one-site adsorption equation which is an expansion of  
 197 the CDE with the addition of a kinetic adsorption member. It is given by

$$\frac{\partial c}{\partial t} = D \frac{\partial^2 c}{\partial z^2} - v \frac{\partial c}{\partial z} - \alpha_{OSA} \left[ (R - 1)c - \frac{\rho_B}{\theta} s \right] \quad \text{Eq. (5)}$$

$$\frac{\rho_B}{\theta} \frac{\partial s}{\partial t} = \alpha_{OSA} \left[ (R - 1)c - \frac{\rho_B}{\theta} s \right] \quad \text{Eq. (6)}$$



198 where  $s$  is the kinetically sorbed concentration to the solid (M), and  $\alpha_{OSA}$  is the first order rate coefficient between dissolved  
199 and adsorbed concentration ( $T^{-1}$ ) which has been found to be a function of pore water velocity and cannot be derived by  
200 batch experiments alone (Nielsen et al., 1986).

201 Following the traditional approach for solute transport parameterization in peat (Rezanezhad et al., 2012, 2017), we initially  
202 assumed the MIM model and compared it with the performance of the CDE for the non-reactive solute. For  $Na^+$ , transport  
203 parameters were additionally estimated with a one-site chemical adsorption model. The data used for the fitting were  
204 averages of three replicates. Parameterization of the model was done with CXTFIT (V2.0; Toride et al., 1995), which  
205 minimises the least-squares. We estimated the following parameters:  $v$  and  $D$  for the CDE,  $v$ ,  $D$ ,  $\beta$ , and  $\alpha_{MIM}$  for MIM, and  
206  $R$  and  $\alpha_{OSA}$  for the OSA model. The estimated  $D$  and  $v$  from the  $Cl^-$  data fit were used for the  $Na^+$  simulations, since  
207 dispersion is a physical material property, and  $R$  can only be determined if  $v$  is fixed from knowledge of a conservative  
208 solute experiment. Using various starting values, we ensured that the global minimum was found. CXTFIT calculates the  
209 variance-covariance matrix, which is required for the calculation of the standard errors of the parameters and the parameter  
210 correlation matrix.

211 The root-mean-squared-weighted error (RMSE) was used as an index for model performance calculated for each of the  
212 tested models (Eq. (14) in Weber et al, 2016). The corrected Akaike Information Criterion (AICc; Eq. (2) in Ye et al. 2008)  
213 was used as a method of model comparison where the model with the smallest AICc is to be favoured. It is a statistically  
214 robust and commonly used index to compare models in soil physics (e.g. Weber et al., 2017a).

## 215 2.4 Unsaturated breakthrough experiments and sensitivity analyses

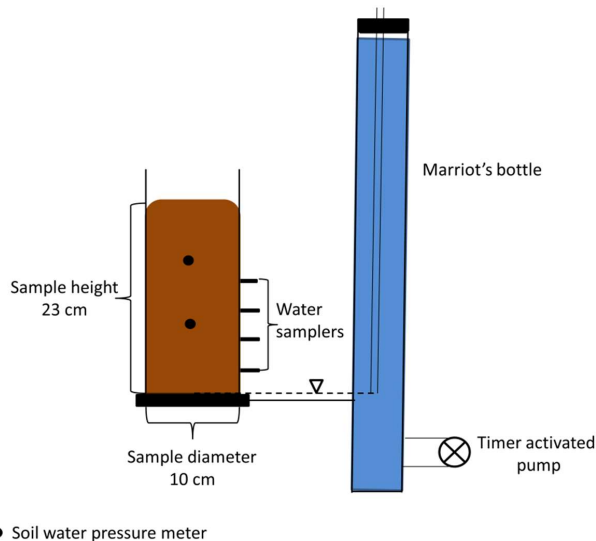
### 216 2.4.1 Sample preparation

217 The unsaturated solute breakthrough experiments were designed as six steady state evaporation columns 23 cm high and 10  
218 cm i.d. (Fig.2). Peat samples were placed in a column constructed with a grooved HDPE base plate with an inlet, a silicon  
219 washer and polypropylene fibre pad, and open at the top (see appendix A.1). The columns were slowly saturated from the  
220 bottom in small increments over 48 hours to minimize trapped gas bubbles. Once saturated, the columns were flushed with 2  
221 column volumes of the NaCl solution to reduce potential changes in hydraulic properties, as previously described. This was  
222 followed by flushing 6 column volumes of ultra-pure water to remove the  $Na^+$  and  $Cl^-$ , with the water overflowing from the  
223 top of the sample. Flushing of  $Na^+$  did not remove all solute, resulting in  $40 \text{ mg l}^{-1}$  of  $Na^+$  remaining in the time 0 samples  
224 taken at the bottom 8 cm of the column. Nevertheless, these concentrations were accounted for in the HYDRUS simulation.  
225 Columns were then drained overnight with 0 cm pressure head at the bottom of the sample, and connected to a Marriot  
226 device containing ultra-pure water. The water table was set to the base of the peat column, and the columns were left to settle  
227 for 11 days, after which the columns were instrumented with the soil tensiometers and water samplers (further details  
228 below).





229 Each Marriot device was fitted with a low flow 12-volt mini water pump to circulate the water within it for 5 minutes every  
230 two hours, to prevent solute stratification. Three Marriot devices were filled with an 8.9 mM solution of NaCl as treatment  
231 and three with ultra-pure water. The columns were fitted with 4 unsaturated soil water samplers at 2.5, 7.5, 12.5 and 17.5 cm  
232 above the water table (19.21.05, Rhizon, Rhizonsphere, Germany), and with 2 two tensiometers at 10 cm (LM) 23 cm (UM),  
233 to determine if the water pressure deviated from hydrostatic conditions (see appendix A.3). Tensiometers were composed of  
234 a porous clay cup and a flexible silicon tube, which was open to the atmosphere. The experiment was run for 120 days;  
235 evaporation was calculated based on changes to the water level in the Marriot device (see appendix A.3). The experiment  
236 was conducted in a room with controlled humidity maintained at ~45%, assisted by a fan to mix the air in the chamber.  
237 Relative humidity (RH) and temperature were measured every 10 minutes (ECT, Decagon, USA) (see appendix A.3).  
238



● Soil water pressure meter

239  
240 **Figure 2 – Unsaturated column experiment column and water reserve setup.**

241  
242 NaCl solution was introduced at the base of the column and drawn upwards by evaporation. Marriot devices were attached to  
243 supply water over the bottom boundary for each column. The pressure head at the lower boundary was fixed to a pressure  
244 head of 0 cm for the duration of the experiment. Daily measurements of the water level in the Marriot were measured with a  
245 measuring tape, and the evaporative water flux over the upper boundary was calculated by dividing the water lost by the  
246 surface area of the column (see appendix A.3).



247 Pore-water samples were taken weekly from each sample height through the Rhizon samplers. On average, 5.5 ml of water  
248 was drawn from each sampler using a dedicated 30 ml polypropylene syringe (Z683647, Sigma-Aldrich, USA). To ensure  
249 equal pull on each sampling point, 6x4x4 cm HDPE spacers were fabricated and placed within the syringe body and piston.  
250 Only samples from time steps 0, 21, 42, 63, 84 and 120 days were analysed. After the experiment ended the cores were  
251 frozen then sliced to ~2 cm thick sections using a band saw. Sections were measured with callipers, weighed and placed in  
252 pre-weighed, food grade and heat resistant bags. The slices were then thawed and ultra-pure water, twice the weight of the  
253 slice, was added to extract the solutes and placed on a table shaker (MaxQ 3000, Thermo scientific) for 48 hours. All  
254 samples were frozen until analysed for  $\text{Na}^+$  and  $\text{Cl}^-$  via IC at the Biogeochemistry Laboratory at the University of Waterloo  
255 (DIONEX ICS 3000, IonPac AS18 and CS16 analytical columns). Results were adjusted to account for the dilution effect of  
256 the added water.

#### 257 **2.4.2 Numerical simulations and sensitivity analyses**

258 The steady state unsaturated evaporation experiment with solute transport was simulated with HYDRUS-1D (Simunek et al.,  
259 2008), which numerically solves the Richard's equation for water flow, and the solute transport equations. For the water  
260 flow, the soil hydraulic properties are the necessary input and were parameterized with a unimodal van Genuchten-Mualem  
261 equation using data collected in the tension disk experiments and transient evaporation experiments. The model domain  
262 represented the 23-cm high column with a spatial discretization of 0.5 cm.

263 The lower boundary condition for the water flow was a constant zero pressure representing the water table. The upper  
264 boundary condition was a flux boundary based on measured evaporation rates. For the solute transport, the lower boundary  
265 was a fixed concentration in the liquid phase and the upper boundary condition was a zero flux. To account for the soil  
266 solution sampling (that would otherwise lead to a misrepresentation of water flow and solute transport), we used the Root  
267 Water Uptake function in HYDRUS by specifying an individual root at the height of each of the four Rhizon samplers. The  
268 applied root water uptake model (Feddes et al., 1978) assumes no salinity stress, no pressure dependent reduction of given  
269 water uptake quantity, and a quasi-infinite maximum allowed concentration for passive root solute uptake. The total water  
270 volume extracted per sampling day was taken to be equal at each root node.

271 Dispersion is dependent on the average linear velocity, which in turn is dependent on the water content (Perkins and  
272 Johnston, 1963). To date, HYDRUS does not account for a water content dependency of dispersion ( $D(\theta)$ ) in solute  
273 transport modelling. Also, this information is not available from the saturated experiment. Therefore, a sensitivity analysis of  
274  $D$  on the model response was done to approximate its quantitative influence on the solute transport. To gauge the range of  
275 values for the sensitivity analysis, a calculation of the change in  $D$  was performed using data gathered from the unsaturated  
276 columns. The calculation used the equation for  $D$  in capillary flow under unsaturated conditions in soils as a function of  $v$  by  
277 Fried and Combarous (1971) (not shown). The equation connects  $D$  to changes in water content and allows the calculation  
278 of changes in  $D$  due to measured changes in water content. Comparison of the calculated values provided with a range of



279 change in D. Calculations indicated that the change in D ranged from 8% to 15%. Therefore, to add extra range the  
 280 sensitivity analysis for the HYDRUS model was performed using  $\pm 20\%$  and a  $\pm 100\%$  change in D.

281

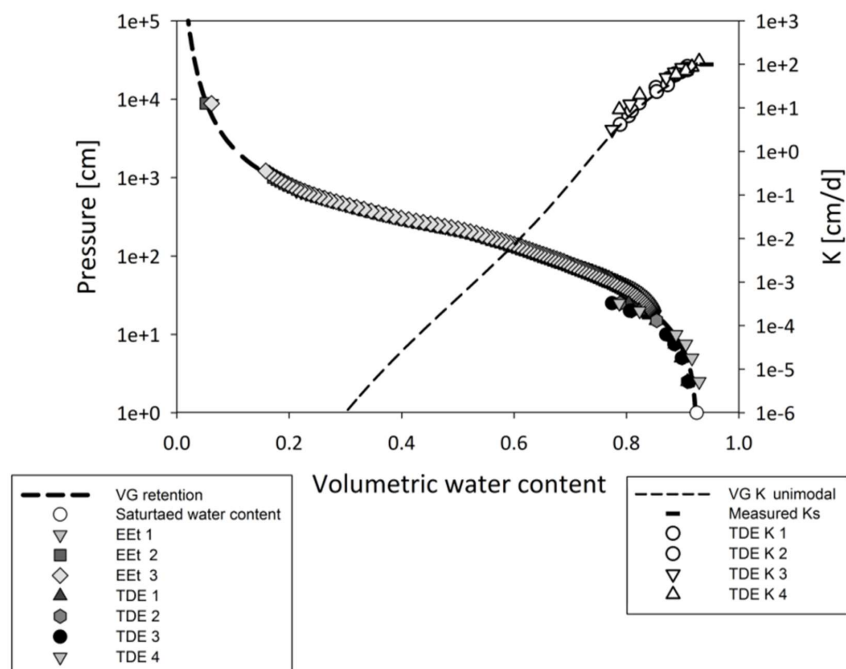
## 282 3 Results and discussion

### 283 3.1 Soil physical properties

284 The bulk density and porosity of the peat used in the various experiments was similar (Table 1). The retention curve (Fig. 3)  
 285 does not have the classical shape that would point at discrimination between an active and inactive porosity (Rezanezhad et  
 286 al., 2016, Weber et al., 2017b). Measured water retention and hydraulic conductivity data closely fit the van Genuchten-  
 287 Mualem unimodal model with an RMSE of 0.03 and AICc value of -342 (Fig. 3; Table 2). Furthermore, the estimated Ks  
 288 value of the unimodal fit ( $106 \text{ cm d}^{-1}$ ; Table 2) is similar to the measured value ( $100 \text{ cm d}^{-1}$ ; Table 1).

289 **Table 1 - Soil physical and hydraulic properties of prepared peat cores from different experiments. Values are averages;**  
 290 **percentages in brackets are the coefficient of variation. Porosity was calculated using particle density from Ketcheson et al. (2017).**

Type of experiment	n	$\rho_B$ [g cm <sup>-3</sup> ]	K <sub>s</sub> [cm d <sup>-1</sup> ]	Porosity [-]
Saturated breakthrough	3	0.12 (1.7%)	99.7 (2.1%)	0.93 (1.3%)
Unsaturated columns	6	0.12 (4.1%)		0.93 (2.8%)
Retention	4	0.12 (3.3%)		0.93 (2.3%)



291

292 Figure 3 – Soil water retention and hydraulic conductivity curves with measurement results of the transient evaporation  
 293 experiments (EEt) and Tension Disk Experiments (TDE) and parameterizations for the unimodal van Genuchten-Mualem model.  
 294 Negative pressure was used for the retention experiment.

295 Table 2– Parameter results for the soil hydraulic properties function of the unimodal model saturation function; the parameter  
 296 names are explained in the text.

model	$\theta_r$	$\theta_s$	$a_1$	$n_1$	$K_s$	$\tau$	$w_2$	$a_2$	$n_2$	$n_p$	RMSE $\theta$ (h)	RMSE $\log_{10} K(h)$	AICc
	[-]	[-]	[cm <sup>-1</sup> ]	[-]	[cm d <sup>-1</sup> ]	[-]	[-]	[cm <sup>-1</sup> ]	[-]	[-]	[-]	[cm d <sup>-1</sup> ]	[-]
uni	0	0.93	0.015	1.6	106	10	-	-	-	5	0.03	0.19	-342

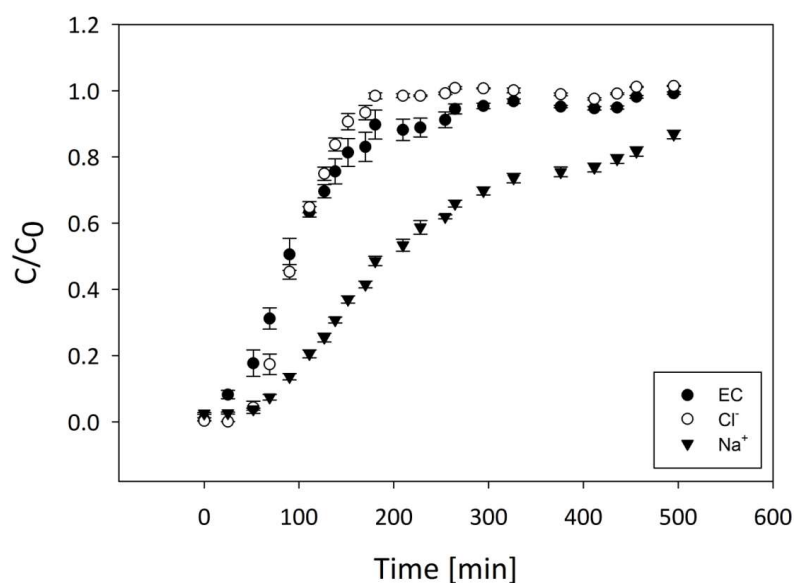
297

### 298 3.2 Saturated breakthrough experiment

299 Cl<sup>-</sup> breakthrough started around ~60 minutes with C/C<sub>0</sub>=0.5 arriving 97 minutes from the start of the experiment  
 300 (Fig. 4). Complete Cl<sup>-</sup> breakthrough (C/C<sub>0</sub>=1) was achieved after 300 min. Similar to Cl<sup>-</sup>, initial Na<sup>+</sup> breakthrough began ~60  
 301 minutes from the start of the experiment (Fig. 4). However, C/C<sub>0</sub>=0.5 was not achieved until ~250 minutes, with only ~0.85  
 302 breakthrough at the end of the experiment that had prolonged tailing, indicating non-equilibrium process. The EC curve is



303 similar in shape to that of  $\text{Cl}^-$ , but took longer to reach the full breakthrough. Attenuation of  $\text{Na}^+$  compared to  $\text{Cl}^-$  is evident  
304 by the greater time until  $C/C_0=0.5$  (Fig. 4), is attributed mainly to the high adsorption capacity of peat (Ho and McKay,  
305 2000). In contrast,  $\text{Cl}^-$  attenuation in peat is mainly due to mechanical dispersion and diffusion into dead-end pores and not  
306 adsorption (Price and Woo, 1988). The dissimilarity of the EC breakthrough curve to that of  $\text{Na}^+$  (Fig. 4) demonstrates the  
307 limitation of using EC as an indicator for reactive solutes. This limitation is due to enrichment of ions in the solution from  
308 the soil and cation exchange with the medium, which changes the solution concentration of the cation of interest; therefore,  
309 EC can be a good estimator for non-reactive solutes but is limited as an indicator for cation transport (Olsen et al., 2000;  
310 Vogeler et al., 2000).



311

312 **Figure 4 – EC,  $\text{Cl}^-$  and  $\text{Na}^+$  corrected saturated breakthrough curves in saturated peat over time. Each point is an average of 3**  
313 **samples, error bars are standard error of mean. Errors were not accounted for in the fitting.**

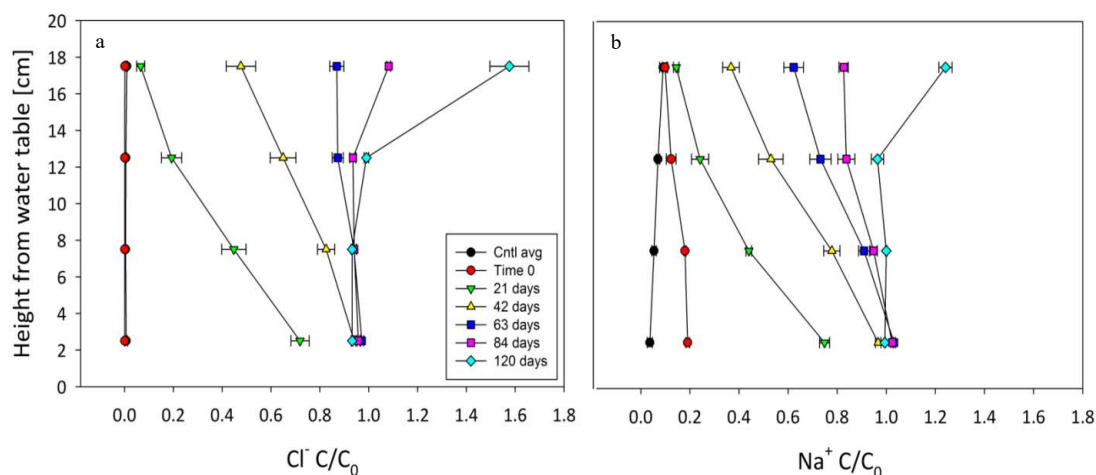
314

### 315 3.3 Unsaturated column experiment

316 The evaporation rate of the experiment was  $3 \text{ mm d}^{-1}$  (not shown, see appendix A.3). As expected,  $\text{Cl}^-$  was transported faster  
317 than  $\text{Na}^+$  as evident by the more rapid rise of  $\text{Cl}^-$  in the peat profile (Fig. 5).  $C/C_0=0.5$  of  $\text{Cl}^-$  reached 7.5 cm above water



318 table within 21 days (Fig. 5a) and by 42 days  $C/C_0=0.5$  reached 17.5cm (Fig. 5a). Complete breakthrough ( $C/C_0=1$ ) of  $\text{Cl}^-$   
 319 was achieved between 63 to 84 days from start of experiment (Fig. 5a).



320

321 **Figure 5 - Breakthrough curves of solutes in the unsaturated columns profile, a) of  $\text{Cl}^-$ , and b) of  $\text{Na}^+$ . Values presented are**  
 322 **averages and whiskers are standard errors. "Cntl avg" represents the average of control measurements; for this aim, all**  
 323 **measurements in a specific height were averaged with each point representing 18 measurements. For the treatment, each point is**  
 324 **an average of 3 measurements. Each treatment curve represents a different sampling time from start of experiment. 0 cm is the**  
 325 **water table location.**

326 Comparably,  $\text{Na}^+ C/C_0=0.5$  reached 7.5 cm within 21 days (Fig. 5b). After 42 days, the  $C/C_0=0.5$  was located between 12.5  
 327 to 17.5 cm from the water table (Fig. 5b). Complete  $\text{Na}^+$  breakthrough occurred later than  $\text{Cl}^-$ , sometime after 84 days but  
 328 before 120 days (Fig. 5b). The accumulation of both elements above inflow concentrations ( $C/C_0>1$ ) at 17.5cm after 120  
 329 days (Fig. 5b), indicates evaporative accumulation occurred as water molecules left the column while solute molecules  
 330 remained (Tsyppkin, 2003). Therefore, evaporative accumulation enhances the breakthrough rate as ions remain in the soil  
 331 while water evaporates; thus, producing a faster accumulation rate than if the breakthrough was estimated using a saturated  
 332 flow system where the solutes would leave the system with the solution. Nevertheless, this effect is a basic product of  
 333 evaporation controlled transport (Elrick et al., 1994; Tsyppkin, 2003).

### 334 3.4 Simulations

#### 335 3.4.1 Solute transport model selection

336 For all transport models, the fitted parameters and associated uncertainties, AICc, and RMSE values are given in Table 3.

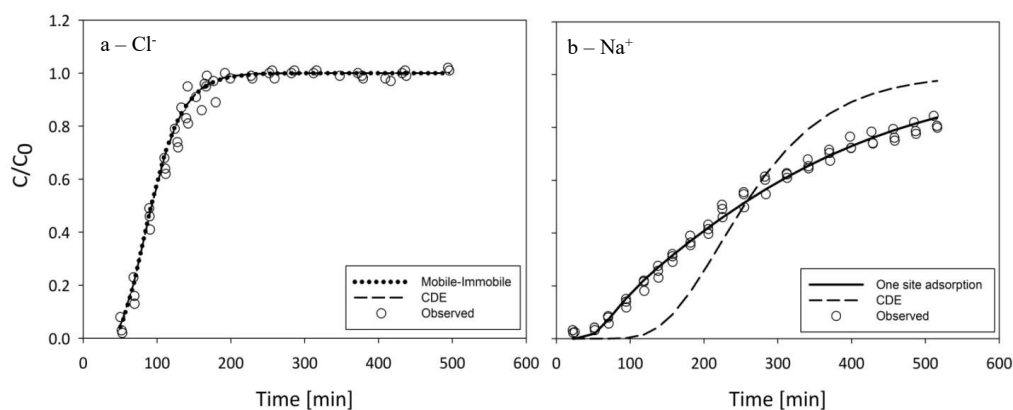
337 The CDE and MIM model for  $\text{Cl}^-$  fit the data well (Fig. 6a), and have identical RMSE (0.032 mg/l). However, the AICc is



338 favors the CDE. Additionally, the MIM model estimated parameters ( $v$ ,  $D$  and  $\beta$ ) show much larger coefficients of variation,  
339 with  $\beta$  varying by 1510% (Table 3). During fitting,  $\alpha_{MIM}$  ran into the CXTFIT internal upper boundary, further suggesting  
340 that the application of the MIM is an over-parameterization and therefore not suitable. Also, the MIM has two additional  
341 parameters than the CDE model, which makes the simpler CDE model preferable (Cavanaugh 1997).

342 The Peclet number for the fitted  $\text{Cl}^-$  breakthrough data, which is the ratio of advective vs diffusive transfer, was 33.9. In  
343 systems with values  $> 2$  diffusion is considered negligible (Huysmans and Dassargues, 2005). Moreover, with  $\beta \rightarrow 1$  (Table  
344 3), the Damköhler number,  $D_d$  approaches infinity, so that the equilibration between the mobile and immobile zones is  
345 considered instantaneous (Wehrer and Totsche, 2005; Vanderborght et al., 1997). In other words,  $D_d$  indicates the system is  
346 not governed by physical non equilibrium processes, but rather the simpler CDE concept applies. The significance of this is  
347 that the physical non-equilibrium approach may be excluded for these samples and boundary conditions. One reason for this  
348 finding could be based on the inherent nature of the samples. The peat of the Nikanotee Fen watershed was moderately  
349 decomposed sedge peat containing small amounts of *Sphagnum* moss (Nwaishi et al., 2015). It is the *Sphagnum* mosses that  
350 contain the hyaline cells (Hayward and Clymo, 1982), which are probably the main cause for the existence of dead end  
351 pores. Therefore, with only a small part of the peat originating from *Sphagnum*, the potential for dead end pores was small  
352 compared to peat that originates mainly from *Sphagnum* moss. Additionally, evidence found in the SEM scans of the peat  
353 used in this study (Fig. 1), shows that the cell walls have decayed, with only the skeleton of the cell remaining, while the  
354 skeleton itself is still intact so water can move much more freely through these structures. These results contradict the  
355 hitherto assumption that solute transport in peat has to be simulated using the MIM. Additionally, this is reflected in the fact  
356 that a multimodal retention curve was not observable, which would have been indicative for a two domain flow of solute  
357 transport.

358 As the CDE model provides a good description of the saturated  $\text{Cl}^-$  breakthrough, and physical non-equilibrium can be  
359 discarded as the underlying process (Table 3; Fig. 6b). Therefore, the non-equilibrium effect observed in the  $\text{Na}^+$   
360 breakthrough (Fig. 6b), must be due to chemical processes such as an interaction of  $\text{Na}^+$  ions with negatively charged sites  
361 on the peat surface whether through retardation or adsorption. Having shown that the MIM is not parsimonious in its  
362 parameters and the robust estimates of  $v$  and  $D$  for the CDE, these were fixed when fitting the remaining model parameters  
363 of the CDE and one-site adsorption model for  $\text{Na}^+$ . First, the CDE was fitted with  $R$  to the  $\text{Na}^+$  data; the resulting curve  
364 shows that equilibrium adsorption does not fit (Fig. 6b). In comparison, the one-site adsorption model fit well (Fig. 6b) and  
365 had a lower RMSE and a considerably lower AICc value (Table 3). Based on the estimated R-value of the one-site  
366 adsorption model, the  $K_d$  value of  $\text{Na}^+$  was  $15.6 \text{ l kg}^{-1}$ . The parameters from the CDE for  $\text{Cl}^-$  and from one-site adsorption for  
367  $\text{Na}^+$  were then used for the HYDRUS simulation of the unsaturated columns.



368

369 **Figure 6 –Breakthrough curves of observed values and fitted models. a) of Cl<sup>-</sup> ; b) of Na<sup>+</sup>.**

370

371 **Table 3 – Estimated saturated transport parameters and the models' goodness of fit data. N.A. = not applicable. Estimated values**  
 372 **are presented with coefficient of variation as percentages in brackets, the parameters are explained in the text.**

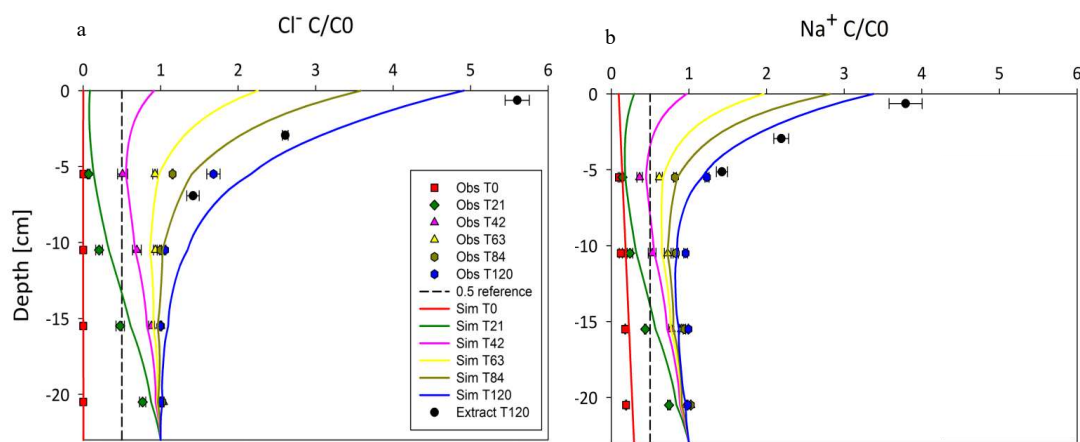
Solute	Model	$v$ ( $\text{cm min}^{-1}$ )	$D$ ( $\text{cm}^2 \text{min}^{-1}$ )	$R$ -	$\beta$ -	$\alpha$ ( $\text{min}^{-1}$ )	RMSE ( $\text{mg l}^{-1}$ )	AICc (-)
Cl <sup>-</sup>	MIM	$9.81 \cdot 10^{-2}$ (91%)	$6.66 \cdot 10^{-2}$ (19%)	fixed to 1	1.00 (1510%)	$6.05 \cdot 10^{-1}$ (0%)	0.032	-406
	CDE	$9.79 \cdot 10^{-2}$ (1%)	$6.66 \cdot 10^{-2}$ (7%)	fixed to 1	N.A.	N.A.	0.032	-408
Na <sup>+</sup>	CDE	fixed	fixed	2.65 (3%)	N.A.	N.A.	0.145	-229
	OSA	fixed	fixed	3.07 (1%)	N.A.	$6.71 \cdot 10^{-4}$ (3%)	0.024	-443

373

### 374 3.4.2 Unsaturated column simulations and sensitivity analyses

375 The HYDRUS predictions of solute concentrations at the four observation points were good for both solutes (Fig.  
 376 7), even though the solute transport model parameterization was based on the saturated experiments. Plotting of the  
 377 concentrations from the solute extractions for the upper part of the core at the end of the experiment reaffirmed the models'  
 378 generally good fit for both solutes (Fig. 7), although in both cases the models underestimate the measured concentration at  
 379 the very top of the soil profile (Table 4).





380

**Figure 7 - Observed values (Obs) from the unsaturated column experiment vs simulated values (Sim) of a)  $\text{Cl}^-$ ; and b)  $\text{Na}^+$ . Observed values are averages and standard error,  $n=3$ . T stands for time and the number that follows is the number of days. Extract T120 represents values measured via extraction as part of post experiment processing. Zero (0) depth marks the surface of the column. Dashed reference line marks  $C/C_0=0.5$ .**

381

382



383 **Table 4 - Unsaturated transport parameters used in or estimated by HYDRUS and models' goodness of fit data. -- = not**  
 384 **applicable. Estimated values are presented with the coefficient of variation as percentages in brackets. Diff. W is the molecular**  
 385 **diffusion coefficient of the solutes.**

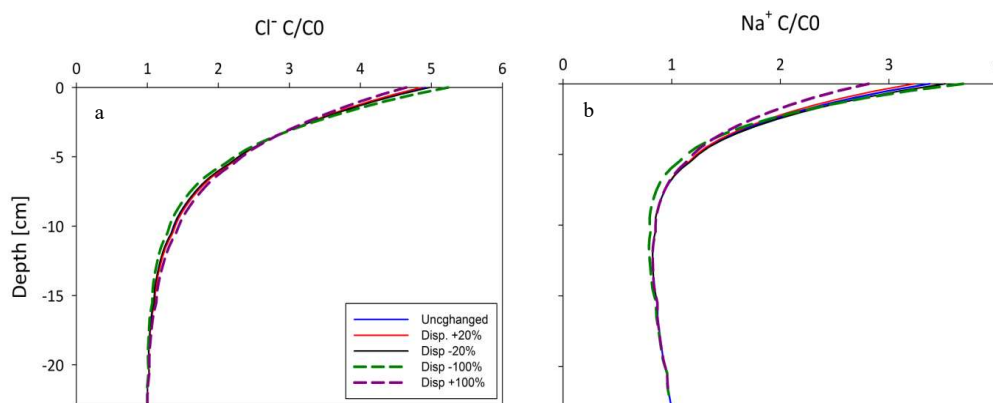
	D [cm <sup>2</sup> min <sup>-1</sup> ]	Kd [l kg <sup>-1</sup> ]	*Diff.W [cm <sup>2</sup> min <sup>-1</sup> ]	α [l min <sup>-1</sup> ]	β	RMSE [mg l <sup>-1</sup> ]
Cl <sup>-</sup>	6.81*10 <sup>-2</sup>	0	1.22*10 <sup>-4</sup>	--	--	15.65
Na <sup>+</sup>	6.81*10 <sup>-2</sup>	15.6	7.98*10 <sup>-5</sup>	1.11*10 <sup>-2</sup> (1.1%)	1.00 (8.1%)	10.19

\* taken from Appelo & Postma (2004).

386

387 Given that the dispersion coefficient for the unsaturated modeling was based on measurements in the saturated flow-through  
 388 chambers, a sensitivity analysis was performed with HYDRUS to determine its impact on the simulations. It indicates that a  
 389 ±20% change in the dispersion coefficient resulted in a ±1.2% and a ±4.1% change in the final concentration of Cl<sup>-</sup> and Na<sup>+</sup>,  
 390 respectively (Fig. 8). Further, an analysis with a ±100% change in D altered the final concentrations by -5% to 6.5% for Cl<sup>-</sup>  
 391 and by 9% to -17% for Na<sup>+</sup>. The analysis demonstrates unsaturated transport is not highly sensitive to changes in the  
 392 dispersion coefficient under the experimental conditions used. Furthermore, since the differences in water contents were not  
 393 large, ranging between 0.93 at full saturation to 0.84 at the top of the column, it is likely that the actual hydrodynamic  
 394 dispersion did not vary significantly.

395



396

397 **Figure 8 – Sensitivity analysis of unsaturated transport for changes in the dispersion coefficient. a) in Cl<sup>-</sup> transport, b) in Na<sup>+</sup>.**

398



### 399 **Conclusions**

400 Saturated breakthrough experiments on disturbed peat, sampled from the Nikanotee Fen, were conducted in the laboratory  
401 using conservative and reactive solutes. With this we tested if the common assumption of mobile-immobile solute transport  
402 process best reflects the transport processes in saturated and unsaturated peat. Based on inverse modelling of time series of  
403 measured conservative tracer concentrations, and robust statistical evaluation, we found that the MIM model was an over-  
404 parameterization for  $\text{Cl}^-$ , since very good results were found using the simpler CDE.

405 For this reason, it could be deduced that the  $\text{Na}^+$  attenuation, expressed by prolonged tailings in the observed breakthrough in  
406 the fen peat is chemically based, as the physical non-equilibrium (i.e. MIM) approach would have had an effect on both  
407 solutes. Hence, we can conclude that  $\text{Na}^+$  showed distinct chemical non-equilibrium adsorption process, which could be  
408 described using the OSA model, and still fulfilling the requirement of parsimony. The results are in contrast to the  
409 commonly accepted MIM behavior of solutes breakthrough in peat samples.

410 The significance of this is that while reactive solutes may be heavily attenuated in peat, conservative solutes are not  
411 necessarily retarded (Hoag and Price, 1997). In this case the degraded structure of the peat (Fig. 1) eliminated many of the  
412 enclosed spaces commonly visible in less decomposed *Sphagnum* peat (see Hoag and Price, 1997; Rezanezhad et al., 2016).  
413 Measured water retention data was adequately described using a unimodal expression for the underlying pore size  
414 distribution, corroborating the finding that a physical dual porosity structure was not present.

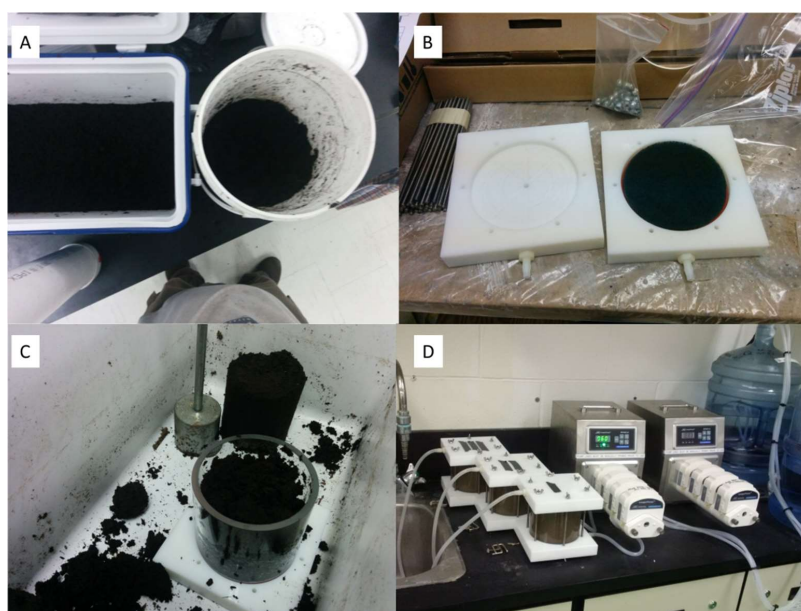
415 On a side note, we can attest that the use of EC as an indirect measurement for a reactive solute will result in overestimation  
416 of breakthrough if the solute interacts with the solid phase.

417 This research implies that automatically assuming mobile and immobile regions in peat is incorrect. The sedge peat with  
418 remnants of *Sphagnum* moss used in this experiment potentially had a limited amount of dead end pores, due to the low  
419 content of *Sphagnum* moss with hyaline cells. Furthermore, evidence suggests that the peat used has decayed enough to lose  
420 the cell walls but not enough to break the cell skeleton, and is likely why the peat lacks the classically assumed MIM  
421 regions. The decomposition may have been enhanced by aeration of the peat in the donor fen (Nwaishi et al., 2015).  
422 Additionally, it is concluded that transport parameters gathered in saturated breakthrough experiments can be used to  
423 simulate transport in slightly unsaturated media under near steady state conditions. Data gathered show that the accumulation  
424 of solutes via evaporation causes concentration to rise quickly above the initial concentration. While these results are valid  
425 for the described boundary conditions and initial conditions, the fate of salt accumulation is not clear under more natural  
426 conditions such as complex meteorological evapotranspiration-precipitation cycles, with, for example, surface inundation  
427 and overland flow export of solutes. Additionally, different salt concentration levels at the lower boundary of the experiment  
428 were not investigated, which has been documented in the case of the Nikanotee Fen watershed (Kessel, 2016). As a first  
429 assessment of the effect  $D$  has on salt accumulation, a synthetic parameter sensitivity analyses was carried out for  $\text{Na}^+$ . To  
430 further understand the rates of the evaporative accumulation, more complex numerical transport model should be used,  
431 including flushing due to precipitation and runoff, using the parameters reported in this study along with various weather



432 scenarios. Considering the complex hydraulic retention and conductivity properties of *Sphagnum* mosses and peat, it is  
433 conceivable that a wide range of tested water contents could affect the choice of the underlying transport process.  
434 Additionally, the experiment was carried out under steady state conditions, unlike the complex meteorological patterns in the  
435 field. Finally, the implications for reclamation projects are that if one of the goals is to enhance solutes attenuation, the origin  
436 and composition of the peat, its water retention properties along with its decomposition state should be characterized as not  
437 all peats will perform equally. From the industry perspective, choosing and peat with dead end pores would allow a potential  
438 for significant attenuation.  
439

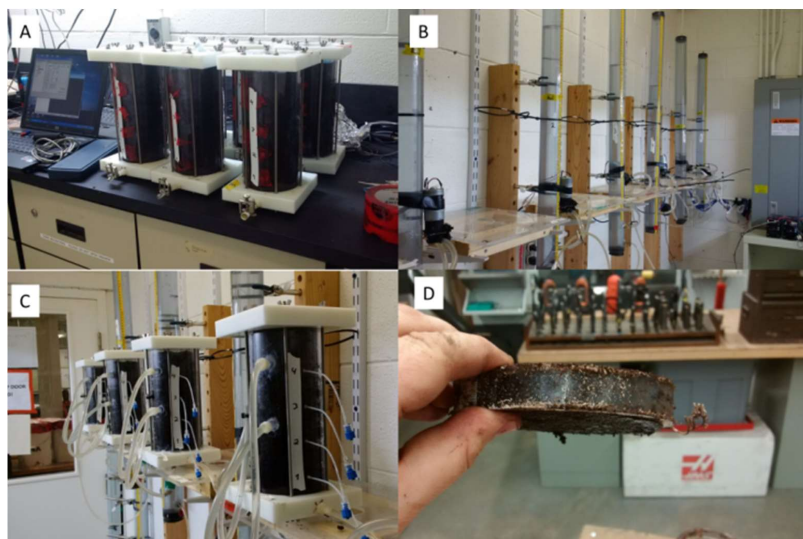
#### 440 A.1 Appendix 1: Pictures of saturated and unsaturated experiments.



441

442 Figure A.1.1 - Pictures from saturated transport experiment. A) Cleaning and mixing the peat; B) flow through cells plates. The  
443 green pad is below the sample, redistributing the water beneath it; C) packing cell with peat; and D) flow through experiment  
444 setup, cells are connected to a pump drawing the solution from a container on a magnetic stirrer.

445



446

447 **Figure A.1.2 - Pictures from the unsaturated transport experiment. A) columns with peat, note the laptop for scale; B) Marriot**  
448 **bottles and pumps; C) columns connected and instrumented, Blue caps are the soil pore water samplers, large tubes are the**  
449 **tensiometers; and D) slice of a peat column before extraction at end of experiment.**

450

## 451 **A.2 Appendix 2: Soil hydraulic properties**

452 Measurements of water retention properties

453 The tension disk experiment (TDE) was conducted on 10 cm i.d. and 5 cm high peat samples at seven different pressure  
454 steps under unsaturated unit gradient vertical flow conditions using a tension disk apparatus that used 15  $\mu\text{m}$  Nytex screens  
455 to prevent air entry below the air entry pressure ( $\sim 35$  cm) (Price et al., 2008, McCarter et al., 2017). Samples were initially  
456 saturated for 48h and two layers of cheese-cloth covered the top and bottom of the sample to maintain the integrity of the  
457 surfaces. The pressure steps ( $h$ ; cm) were -2.5, -5, -7.5, -10, -15, -20, -25 cm, which was also the order in which the  
458 experiment was conducted. During the experiment, outflow was monitored for each pressure step by a scale with an accuracy  
459 of at least 0.1 g and logged at 1-minute intervals. The experiment stopped when there was no change from past  
460 measurements over a 30-min. period. After each step the weight of the sample was determined to enable calculation of the  
461 water content. From the outflow, the unsaturated hydraulic conductivity was calculated from the Darcy-Buckingham  
462 equation (Swartzendruber, 1969).

463 **Saturated hydraulic conductivity**



464 The FTC were used for the determination of the saturated conductivity ( $K_s$ ; cm d<sup>-1</sup>), too, which were connected to a  
 465 Marriot's bottle supplying a constant pressure head. The adopted method was a constant head test (Freeze and Cherry, 1979)  
 466 with a gradient of 0.44. Once the outflow stabilized, it was measured in a 250ml glass graduated cylinder (S63459, Fischer  
 467 Scientific, USA) every 2 min over 20 min.

#### 468 **Transient evaporation experiment**

469 The transient evaporation experiment (EET) was conducted on the same samples as the TDE. With a 0 cm pressure head at  
 470 the bottom prior to the beginning of the EET with the commercial UMS HYPROP device (UMS GmbH, Munich, Germany).  
 471 The samples had a larger diameter than the UMS HYPROP device so that Plexiglas screens were used at the bottom to seal  
 472 and prop the sample. The pressure head was directly measured in the middle of the sample and, thus, directly related to the  
 473 calculated water content to obtain the retention information, which is a valid approximation at or near a linear pressure  
 474 distribution (Becher, 1971). With this, the evaluation for conductivity is not reliable.

#### 475 **Inverse fitting of soil hydraulic properties**

476 The water retention and unsaturated hydraulic conductivity data were used to parameterize soil hydraulic property (SHP)  
 477 models. We used the unimodal van Genuchten-Mualem model combination (van Genuchten, 1980; Mualem, 1976). We used  
 478 the analytical expression derived by Priesack and Durner (2006). The soil water retention function is given by

$$\theta(h) = \theta_r + (\theta_s - \theta_r) \Gamma(h) \quad \text{Eq.(A.1)}$$

479 where  $\theta_r$  is the residual and  $\theta_s$  the saturated water content (cm<sup>3</sup> cm<sup>-3</sup>) and  $\Gamma(h)$  (-) the effective saturation given by

$$\Gamma(h) = \sum_{i=1}^k \Gamma_i(h) = \sum_{i=1}^k w_i [1 + (-\alpha_i h)^{n_i}]^{m_i} \quad \text{Eq.(A.2)}$$

480 where,  $w_i$  is a weighting coefficient between the modal pore size distributions, and  $\alpha_i$  (cm<sup>-1</sup>) and  $n_i$  (-) are shape parameters  
 481 with constraining,  $m_i = 1 - 1/n_i$ . The unimodal van Genuchten saturation function is obtained by  $k = 1$ . The unsaturated  
 482 hydraulic conductivity is expressed as

$$K(\Gamma) = K_s \Gamma^\tau \left( \sum_{i=1}^k w_i \alpha_i \right)^{-2} \left( \sum_{i=1}^k w_i \alpha_i [1 - (1 - \Gamma)^{1/m_i}]^{m_i} \right)^2 \quad \text{Eq.(A.3)}$$

483 where  $K_s$  is the saturated hydraulic conductivity (cm d<sup>-1</sup>) and  $\tau$  is sometimes referred to as a tortuosity constant, which  
 484 should be positive-

485 All parameters were estimated except for  $\theta_s$ , which was set to 0.925, i.e. the porosity value. Estimation was done in R.3.2.1  
 486 (R Core Team 2015) with implementation of the differential evolution optimiser to minimise the sum of squared errors for  
 487 the retention and hydraulic conductivity curves (Mullen et al., 2011). The estimation of the soil hydraulic properties of the  
 488 fen peat by inverse estimation was done as described in Peters and Durner (2008). After all procedures were concluded, bulk  
 489 densities for all samples were determined gravimetrically based on an oven-dry mass basis for samples dried at 80 °C until  
 490 no difference in weight was measured (Gardner, 1986). From knowledge of the dry weight and experimental system weight  
 491 water contents could be calculated for the soil hydraulic properties.



492 Statistical parameters

493 The root mean square error (RMSE) is used as a metric to describing the model prediction quality, such that

$$RMSE = \sqrt{\frac{1}{m} \sum_{l=1}^m (y_l - \hat{y}_l)^2} \quad \text{Eq.(A.4)}$$

494

495 where  $m$  is the number of observations,  $y_l$  is the observed and  $\hat{y}_l$  the model predicted value (solute concentration, water  
496 content or hydraulic conductivity). The corrected Akaike Information Criterion (AICc; Ye et al. 2008)) was also used as a  
497 method of model comparison where the model with the smallest AICc is to be favored. Applications so soil hydrological  
498 model testing can be found in Weber et al. (2017a, 2017b).

$$AICc = m \ln \left( \frac{1}{m} \sum_{l=1}^m (y_l - \hat{y}_l)^2 \right) + 2 n_p + 2 \frac{n_p(n_p + 1)}{m - n_p - 1} + C \quad \text{Eq.(A.5)}$$

499 where  $n_p$  is the number of parameters of a respective model.

500 Estimation of model parameters was done by minimising the sum of squared errors for the retention and hydraulic  
501 conductivity curves in R.3.2.1 (R Core Team 2015) with an implementation of the differential evolution optimiser (Mullen et  
502 al., 2011) by adopting the multi-objective function as described in Peters and Durner (2008).

503

504 References (References that do not appear here can be found in the main reference list):

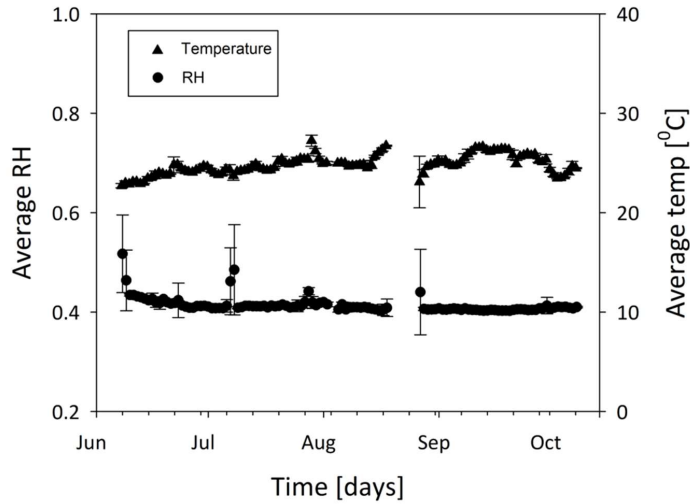
505 Price, J. S., Whittington, P. N., Elrick, D. E., Strack, M., Brunet, N., & Faux, E. (2008). A method to determine unsaturated  
506 hydraulic conductivity in living and undecomposed moss. *Soil Sci. Soc. Am. J.* , 72(2), 487-491.

507

508

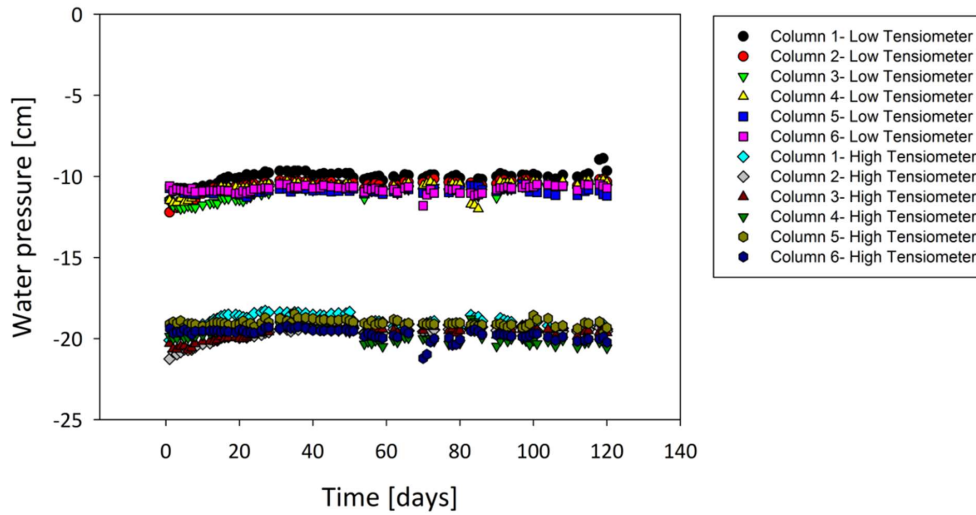
### 509 A.3 Appendix 3: Unsaturated experiment conditions

510 Ambient conditions in the chamber where the experiment was conducted were stable with an average temperature  
511 of  $\sim 25 \pm 1$  °C and an average RH of  $41 \pm 0.02$  % (Fig. A.3.1). Additionally, water pressure profile in the soil did not vary much  
512 for each column; soil water pressure above the water table averaged  $-10.7 \pm 0.5$  cm for the low meter and  $-19.5 \pm 0.5$  cm for the  
513 high meter (Fig. A.3.2). Furthermore, data from all columns were in a similar range (Fig. A.3.2) meaning the columns were  
514 reasonable replicates in soil water pressure.



515

516 Figure A.3.1 – measured temperature and relative humidity during the unsaturated column experiment. Each point is a daily  
 517 average of 144 measurements and corresponding standard error.



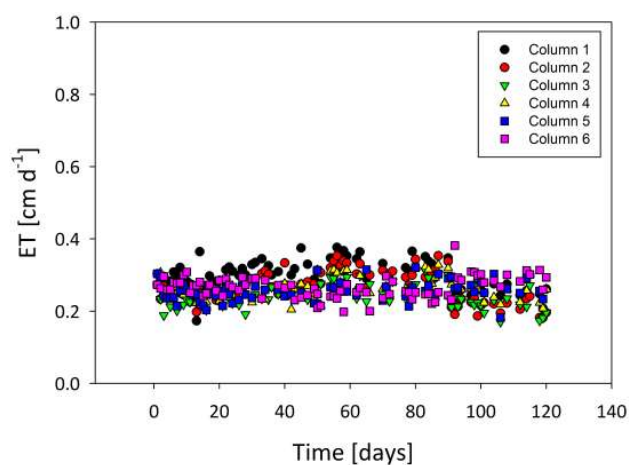
518





519 **Figure A.3.2 – Soil water pressure measurements over time. 0 cm marks the water table. Values around the -10 cm mark are from**  
520 **the low pressure meters of all 6 columns; values around -20cm are from the high pressure meters.**

521 Moreover, E data strengthen the conclusion that the columns were decent replicates with an overall low fluctuation  
522 in values averaging at  $0.27 \pm 0.05 \text{ cm d}^{-1}$  (Fig. A.3.3).



523

524 **Figure A.3.3– Calculated ET during the experiment. Data presented is for each column separately (color coded, see legend).**

525

526

### 527 Acknowledgements

528 Thank you to Harmen Vander Heide, Dan Beaver, Andrew Urschel, Scott Ketcheson, Eric Kessel, Tasha-Leigh Gauthier,  
529 James Sherwood, Corey Wells and Vito Lam for their help in logistic, fabrication and analysis. Additionally, thanks to Dr.  
530 Mazda Kompanizare, Behrad Gharedaghloo and Dr. Fereidoun Rezanezhad, and Dr. SC Iden for their advice. Funding from  
531 the following sources is gratefully acknowledged: Natural Science and Engineering Research Council Collaborative  
532 Research and Development (NSERC-CRD), Suncor Energy Inc., Shell Canada Limited and Esso Imperial Oil Limited, and  
533 the German Academic Exchange Service.

### 534 References

535 Appelo, C. A. J., & Postma, D. (2004). Geochemistry, groundwater and pollution. CRC press.



- 536 Becher, H. H. (1971). Ein Verfahren zur Messung der ungesättigten Wasserleitfähigkeit. *J. Plant Nutr. Soil Sci.*, 128(1), 1-  
537 12.
- 538 Blodau, C., (2002). Carbon cycling in peatlands — A review of processes and controls. *Environmental Reviews*, 10, pp.111–  
539 134.
- 540 Bott, R. (2010). *Canada's Oil Sands* (3<sup>rd</sup> edition). Canadian Center for Energy Information. Calgary, Alberta.
- 541 Cameron, D. R., & Klute, A. (1977). Convective-dispersive solute transport with a combined equilibrium and kinetic  
542 adsorption model. *Water Resour. Res.*, 13(1), 183-188.
- 543 Cavanaugh, J. E. (1997), "Unifying the derivations of the Akaike and corrected Akaike information criteria", *Stat. Probab.*  
544 *Lett.* 31: 201–208.
- 545 Clymo, R.S., (1983). Peat. In: A.J.P. Gore (ed.). *Mires, Swamp, Bog, Fen and Moor, General Studies (Ecosystem of the*  
546 *World 4A)*. Elsevier, Amsterdam, pp. 159-224
- 547 Coats, K. H., & Smith, B. D. (1964). Dead-end pore volume and dispersion in porous media. *Society of petroleum engineers*  
548 *journal*, 4(01), 73-84.
- 549 Daly C, Price JS, Rezanezhad F, Pouliot R, Rochefort L, & Graf M. (2012). Initiatives in oil sand reclamation:  
550 Considerations for building a fen peatland in a post-mined oil sands landscape. In: *Restoration and Reclamation of Boreal*  
551 *Ecosystems -Attaining Sustainable Development*. Vitt D, Bhatti JS (eds.) Cambridge University Press, pp: 179-201.
- 552 Devito, K., Mendoza, C., & Qualizza, C. (2012). Conceptualizing water movement in the Boreal Plains. Implications for  
553 watershed reconstruction. Synthesis report prepared for the Canadian Oil Sands Network for Research and Development,  
554 Environmental and Reclamation Research Group. 164p.
- 555 Elrick, D. E., Mermoud, A., & Monnier, T. (1994). An analysis of solute accumulation during steady-state evaporation in an  
556 initially contaminated soil. *J. Hydrol. (Amst.)*, 155(1), 27-38.
- 557 Feddes, R. A., Kowalik, P. J., & Zaradny, H. (1978). Simulation of field water use and crop yield. Centre for Agricultural  
558 Publishing and Documentation.
- 559 Freeze, R. A., & Cherry, J. A. (1979). *Groundwater* (No. 629.1 F7).
- 560 Fried, J. J., & Combarous, M. A. (1971). Dispersion in porous media. *Adv. Hydrosoci*, 7(169).
- 561 Gardner W.H. (1986). Water Content. In *Methods of Soil Analysis: Physical and Mineralogical 29 Methods*, Kiute A  
562 (Editor). *Agronomy Series 9 (Part 1)*, Soil Science Society of America, 30 Madison, Wisconsin, 493-544.
- 563 Gorham, E., (1991). Northern peatlands e role in the carbon-cycle and probable responses to climatic warming. *Ecol. Appl.*  
564 1, 182-195.
- 565 Government of Alberta. (2015). *Alberta's Oil Sands: Reclamation*. Government of Alberta.  
566 <http://oilsands.alberta.ca/FactSheets/FactSheet-Reclamation-2015.pdf>.
- 567 Government of Alberta. (2016). Alberta regulation 76/88, Oil Sands Conservation Act, oil sands conservation rules. Laws  
568 online catalogue. Online at:



- 569 [http://www.qp.alberta.ca/1266.cfm?page=1988\\_076.cfm&leg\\_type=Regs&isbncln=9780779758876&display=html](http://www.qp.alberta.ca/1266.cfm?page=1988_076.cfm&leg_type=Regs&isbncln=9780779758876&display=html).  
570 Accessed June 29, 2016.
- 571 Ho, Y. S., & McKay, G. (2000). The kinetics of sorption of divalent metal ions onto sphagnum moss peat. *Water Res.*, 34(3),  
572 735-742.
- 573 Hoag, R. S., & Price, J. S. (1997). The effects of matrix diffusion on solute transport and retardation in undisturbed peat in  
574 laboratory columns. *J. Contam. Hydrol.*, 28(3), 193-205.
- 575 Huysmans, M., & Dassargues, A. (2005). Review of the use of Péclet numbers to determine the relative importance of  
576 advection and diffusion in low permeability environments. *Hydrogeol. J.*, 13(5-6), 895-904.
- 577 Iden, S.C. & Durner, W. (2008) Multiple batch extraction test to estimate contaminant release parameters using a Bayesian  
578 approach, *J. Contam. Hydrol.* 95, 168–182.
- 579 Ketcheson, S. J., Price, J. S., & Weber, T. K. D. (2017). Hydrophysical properties of mine reclamation materials (LFH,  
580 tailings sand, petroleum coke and organic peat soils) in a constructed watershed. *International Journal of Mining,*  
581 *Reclamation and Environment*.
- 582 Klute, A., & Dirksen, C., (1986). Hydraulic conductivity and diffusivity: laboratory methods. In: Klute, A. (Ed.), *Methods of*  
583 *Soil Analysis. Part 1. Physical and Mineralogical Methods*, 2nd ed. Agronomy Monograph. 9. ASA, Madison, WI, pp. 687–  
584 734
- 585 Limpens, J., Berendse, F., Blodau, C., Canadell, J. G., Freeman, C., Holden, J., Roulet, T., Rydin, H. & Schaepman-Strub,  
586 G. (2008). Peatlands and the carbon cycle: from local processes to global implications—a synthesis. *Biogeosciences*, 5(5),  
587 1475-1491.
- 588 McCarter, C., Ketcheson, S.J., Weber, T.K.D., Whittington, P.N., Scarlett, S. and Price, J.S. (in press) A modified technique  
589 for measuring unsaturated hydraulic conductivity in Sphagnum moss and peat. *Soil Sci. Soc. Am. J.*, MS# S-2017-01-0006-  
590 OR. Accepted: 10-March-2017.
- 591 Mualem, Y. (1976). A new model for predicting the hydraulic conductivity of unsaturated porous media. *Water Resour.*  
592 *Res.*, 12(3), 513-522.
- 593 Nielsen, D. R., & Biggar, J. W. (1986). Water flow and solute transport processes in the unsaturated zone. *Water Resour.*  
594 *Res.*, 22(9S).
- 595 Nkedi-Kizza, P., Biggar, J. W., Selim, H. M., Van Genuchten, M. T., Wierenga, P. J., Davidson, J. M., & Nielsen, D. R.  
596 (1984). On the equivalence of two conceptual models for describing ion exchange during transport through an aggregated  
597 oxisol. *Water Resour. Res.*, 20(8), 1123-1130.
- 598 Nkedi-Kizza, P., Brusseau, M. L., Rao, P. S. C., & Hornsby, A. G. (1989). Nonequilibrium sorption during displacement of  
599 hydrophobic organic chemicals and calcium-45 through soil columns with aqueous and mixed solvents. *Environ. Sci.*  
600 *Technol.*, 23(7), 814-820.
- 601 Nwaishi, F., Petrone, R. M., Price, J. S., Ketcheson, S. J., Slawson, R., & Andersen, R. (2015). Impacts of donor-peat  
602 management practices on the functional characteristics of a constructed fen. *Ecol. Eng.*, 81, 471-480.



- 603 Olsen, H., Gui, S., & Lu, N. (2000). Critical review of coupled flow theories for clay barriers. *Transportation Research*  
604 *Record: Transp. Res. Rec.*, (1714), 57-64.
- 605 Ours, D. P., Siegel, D. I., & Glaser, P. H. (1997). Chemical dilation and the dual porosity of humified bog peat. *J. Hydrol.*  
606 (Amst.), 196(1), 348-360.
- 607 Passioura, J. B. (1971). Hydrodynamic dispersion in aggregated media: 1. Theory. *Soil science*, 111(6), 339-344.
- 608 Perkins, T. K., & Johnston, O. C. (1963). A review of diffusion and dispersion in porous media. *Society of Petroleum*  
609 *Engineers Journal*, 3(01), 70-84.
- 610 Peters, A., & Durner, W. (2008). A simple model for describing hydraulic conductivity in unsaturated porous media  
611 accounting for film and capillary flow. *Water Resour. Res.*, 44(11).
- 612 Philip, J. R. (1968). Diffusion, dead-end pores, and linearized absorption in aggregated media. *Soil Research*, 6(1), 21-30.
- 613 Price, J.S. & Woo, M.K., (1988). Wetlands as waste repositories? Solute transport in peat. *Proc. Nat. Student Conference on*  
614 *Northern Studies*, 18-19 November 1986, Assoc. of Canadian Universities for Northern Studies, Ottawa, Ont., pp. 392-395.
- 615 Price, J.S., McLaren, R.G. & Rudolph, D.L. (2010). Landscape restoration after oil sands mining: conceptual design and  
616 hydrological modelling for fen reconstruction. *Int. J. Min. Reclam. Environ.*, 24(2), 109–123.
- 617 Price, J.S., L. Rochefort, F. Rezanezhad, R. Pouliot, Martha D. Graf & R. Andersen. (2011). Fen creation in the Athabasca  
618 oil sands region, Final Report and Implications, Suncor Energy Inc., 178 pp.
- 619 Priesack, E., & Durner, W. (2006). Closed-form expression for the multi-modal unsaturated conductivity function. *Vadose*  
620 *Zone J.*, 5(1), 121-124.
- 621 R Core Team: R (version 3.1.2): A language and environment for statistical computing, R Foundation for Statistical  
622 Computing, Vienna, Austria, 2014.
- 623 Rajendran, A., Kariwala, V., & Farooq, S. (2008). Correction procedures for extra-column effects in dynamic column  
624 breakthrough experiments. *Chem. Eng. Sci.*, 63(10), 2696-2706.
- 625 Rezanezhad, F., Price, J.S., & Craig, J.R. (2012). The effect of dual-porosity on transport and retardation in peat: A  
626 laboratory experiment. *Can. J. Soil Sci.*, 92: 1-10.
- 627 Rezanezhad F., Price J.S., Quinton W.L., Lennartz B., Milojevic T. & Van Cappellen P. (2016). Structure of peat soils and  
628 implications for water storage, flow and solute transport: A review update for geochemists. *Chem. Geol.* 419, 75-84.
- 629 Ross, P. J., & Smettem, K. R. (1993). Describing soil hydraulic properties with sums of simple functions. *Soil Sci. Soc. Am.*  
630 *J.*, 57(1), 26-29.
- 631 Rezanezhad F., Kleimeier, C., Milojevic, T., Liu, H., Weber, T.K.D., van Cappellen, P., and Lennart, B.: The role of pore  
632 structure on nitrate reduction in peat soil: A physical characterization of pore distribution and solute transport, *WETLANDS*,  
633 2017, in revision.
- 634 Schindler, U. (1980). Ein Schnellverfahren zur Messung der Wasserleitfähigkeit im teilgesättigten Boden an  
635 Stechzylinderproben, *Arch. Acker- Pflanzenbau Bodenkd.*, 24, 1-7



- 636 Simhayov, R. B., Price, J. S., Smeaton, C. M., Parsons, C., Rezanezhad, F., & Van Cappellen, P. (2017). Solute pools in  
637 Nikanotee Fen watershed in the Athabasca oil sands region. *Environ. Pollut.*, 225, 150-162.
- 638 Šimůnek, J., M. Th. van Genuchten, M. Sejna, N. Toride, & F. J. Leij, (1999). The STANMOD Computer Software for  
639 Evaluating Solute Transport in Porous Media Using Analytical Solutions of Convection-Dispersion Equation, Versions 1.0  
640 and 2.0, U.S. Salinity Laboratory, USDA, ARS, Riverside, California.
- 641 Šimůnek, J., & van Genuchten, M. T. (2008). Modeling nonequilibrium flow and transport processes using  
642 HYDRUS. *Vadose Zone J.*, 7(2), 782-797.
- 643 Šimůnek, J., van Genuchten, M. T., & Šejna, M. (2008). Development and applications of the HYDRUS and STANMOD  
644 software packages and related codes. *Vadose Zone J.*, 7(2), 587-600.
- 645 Skaggs, T. H., & F. J. Leij. (2002). Chapter 6.3: Solute transport: Theoretical background. In *Methods of Soil Analysis: Part*  
646 *4. Physical Methods*, 1353-1380. J. H. Dane and C.G. Topp, eds. Madison, Wisc. SSSA.
- 647 Squires, A.J. (2005). Ecotoxicological assesment of using coke in aquatic reclamation strategies at the Alberta Oil Sands.  
648 M.Sc. thesis. University of Saskatchewan, Saskatoon, Saskatchewan, Canada.
- 649 Swartzendruber, D. (1969). The flow of water in unsaturated soils. *Flow through porous media*. Academic Press, New York,  
650 215-291.
- 651 Toride, N., Leij, F. J., & Genuchten, M. T. (1993). A comprehensive set of analytical solutions for nonequilibrium solute  
652 transport with first-order decay and zero-order production. *Water Resour. Res.*, 29(7), 2167-2182.
- 653 Toride, N., Leij, F. J., & Van Genuchten, M. T. (1995). The CXTFIT code for estimating transport parameters from  
654 laboratory or filed tracer experiments. Riverside: US Salinity Laboratory.
- 655 Tsyppkin, G. G. (2003). Accumulation and precipitation of salts during groundwater evaporation and flow. *Fluid dynamics*,  
656 38(6), 900-907.
- 657 Vanderborght, J., Mallants, D., Vanclooster, M., & Feyen, J. (1997). Parameter uncertainty in the mobile-immobile solute  
658 transport model. *J. Hydrol. (Amst.)*, 190(1), 75-101.
- 659 Van Genuchten, M. T., Davidson, J. M., & Wierenga, P. J. (1974). An evaluation of kinetic and equilibrium equations for the  
660 prediction of pesticide movement through porous media. *Soil Sci. Soc. Am. J.* , 38(1), 29-35.
- 661 Van Genuchten, M. T. (1980). A closed-form equation for predicting the hydraulic conductivity of unsaturated soils. *Soil*  
662 *Sci. Soc. Am. J.* , 44(5), 892-898.
- 663 Van Genuchten, M. T., & Alves, W. J. (1982). Analytical solutions of the one-dimensional convective-dispersive solute  
664 transport equation (No. 157268). United States Department of Agriculture, Economic Research Service.
- 665 Van Genuchten, M. T., & Wagenet, R. J. (1989). Two-site/two-region models for pesticide transport and degradation:  
666 Theoretical development and analytical solutions. *Soil Sci. Soc. Am. J.* , 53(5), 1303-1310.
- 667 Vitt D, Halsey L, Thormann M, & Martin T. (1996). Peatland inventory of Alberta. Phase I: Overview of peatland resources  
668 in the natural regions and subregions of the province., Centre PR (ed.) University of Alberta.



- 669 Vitt, D. H., Halsey, L. A., Bauer, I. E., & Campbell, C. (2000). Spatial and temporal trends in carbon storage of peatlands of  
670 continental western Canada through the Holocene. *Can. J. Earth Sci.*, 37(5), 683-693.
- 671 Vogeler, I., Duwig, C., Clothier, B. E., & Green, S. R. (2000). A simple approach to determine reactive solute transport  
672 using time domain reflectometry. *Soil Sci. Soc. Am. J.*, 64(1), 12-18.
- 673 Wehrer, M., & Totsche, K. U. (2005). Determination of effective release rates of polycyclic aromatic hydrocarbons and  
674 dissolved organic carbon by column outflow experiments. *Eur. J. Soil Sci.*, 56(6), 803-813.
- 675 Weihermüller, L., Siemens, J., Deurer, M., Knoblauch, S., Rupp, H., Göttlein, A., & Pütz, T. (2007). In situ soil water  
676 extraction: A review. *J. Environ. Qual.*, 36(6), 1735-1748.
- 677 Zurmühl, T., & Durner, W. (1996) Modeling transient water and solute transport in a biporous soil, *Water Resour. Res.*, Vol.  
678 32, No. 4, P. 819-829.
- 679 Vrugt, J. A. and Dane, J. H. (2006). Inverse Modelling of Soil Hydraulic Properties. *Encyclopaedia of Hydrological*  
680 *Sciences*. 6:77.
- 681 Weber, T. K. D., Iden, S. C. and Durner, W., 2017a, Unsaturated hydraulic properties of Sphagnum moss and peat reveal  
682 trimodal pore-size distributions, *Water Resour. Res.*, 53(1):415-434.
- 683 Weber, T. K. D., Iden, S. C. and Durner, W., 2017b, Peatland bog pedogenesis is reflected in effective unsaturated hydraulic  
684 properties, *HESSD*, doi: 10.5194/hess-2017-297.